Automated detection of cracks in roads using ground penetrating radar

Eskandari Torbaghan, Mehran; Li, Wenda; Metje, Nicole; Burrow, Michael; Chapman, David; Rogers, Chris

[Link to publication on Research at Birmingham portal](#)

Article type: Research Paper

Title: Automated Detection of Cracks in Roads using Ground Penetrating Radar

Author 1 (Corresponding author)

- **Given name**: Mehran **Family name**: Eskandari Torbaghan, MSc, PhD. Research Fellow
- School of Engineering, Department of Civil Engineering, College of Engineering and Physical Sciences, University of Birmingham, Birmingham, B15 2TT, UK, Tel.: +44-74056-39382, E-Mail: M.eskandaritorbaghan@bham.ac.uk

Author 2

- **Given name**: Wenda **Family name**: Li, MSc, PhD. Research Fellow
- School of Engineering, Department of Civil Engineering, College of Engineering and Physical Sciences, University of Birmingham, Birmingham, B15 2TT, UK, Tel.: + , E-Mail: W.Li@bham.ac.uk

Author 3

- **Given name**: Nicole **Family name**: Metje, Professor of Infrastructure Monitoring, PhD, Dipl.-Ing, MCInstCES, MASCE, FHEA
- School of Engineering, College of Engineering and Physical Sciences, University of Birmingham, Birmingham, B15 2TT, UK, Tel.: +44 (0) 121 414 4182, Email: n.metje@bham.ac.uk

Author 4

- **Given name**: Michael **Family name**: Burrow, MA (Cantab), PhD
- Department of Civil Engineering, College of Engineering and Physical Sciences, University of Birmingham, Birmingham, UK, Email: M.P.Burrow@bham.ac.uk

Author 5

- **Given name**: David N. **Family name**: Chapman, Professor of Geotechnical Engineering, BSc (Hons), DIS, PhD, CEng, MICE, FHEA

- School of Engineering, Department of Civil Engineering, College of Engineering and Physical Sciences, University of Birmingham, Birmingham, B15 2TT, UK, Tel.: +44 (0) 121 414 5150, Email: d.n.chapman@bham.ac.uk

Author 6

- **Given name**: Christopher D.F. **Family name**: Rogers, Professor of Geotechnical Engineering, Eur Ing, BSc, PhD, CEng, MICE, MCIHT
- School of Engineering, Department of Civil Engineering, College of Engineering and Physical Sciences, University of Birmingham, Birmingham, B15 2TT, UK, Tel.: +44 (0) 121 414 5066, Email: c.d.f.rogers@bham.ac.uk

Abstract

A critical assessment criterion for road condition assessment is the amount and severity of cracking. Cracking causes a loss of structural capacity (i.e. strength and stiffness) and if severe can cause water infiltration into the subbase and subgrade, potentially leading to more serious structural failure. The onset of cracking therefore accelerates the processes of deterioration of the road. To date the accurate and reliable automated detection of road surface cracking is still problematic.

Ground Penetrating Radar (GPR) has the potential to detect cracks in materials as they cause changes in electromagnetic reflection. This paper proposes a method of automatic detection of road surface cracks using GPR and establishes the limits of its potential regarding the detectable crack size.

Tests were conducted on asphalt pavement samples in a controlled laboratory environment. Significant changes in diffracted signal levels were observed in the GPR image when the image was analysed using a Singular Value Decomposition (SVD) algorithm for clutter reduction and a median filter to reduce noise. Moreover, a manifestly enhanced performance was achieved using a novel post-processing technique, which enabled the detection of cracks larger than 1.3 mm in width. The detected cracks were detectable irrespectively of the simulated physical conditions suggesting that the developed methodology is robust for use in practice. The experimental results indicate that the GPR system can be applied to automatically detect road cracking reliably in practice.

Keywords:

List of Notation

CNN	Convolutional Neural Network
EM	Electro-Magnetic
FDTD	Finite Difference Time-Domain
GPR	Ground Penetrating Radar
HMA	Hot Mix Asphalt
LiDAR	Light Detection and Ranging
MLS	Mobile Laser Scanning
PCC	Portland Cement Concrete
PSNR	Peak-Signal-to-Noise Ratio
RF	Radio Frequency
RMS	Root-Mean-Square

SNR	Signal-to-Noise Ratio
SVD	Singular Value Decomposition
ToF	Time-of-Flight
TRL	Transport Research Laboratory

1   Introduction

Assessing the condition of the road network is vital for ensuring its continued functionality. In the UK it has been reported that one in five local roads could fail in the next five years, while local roads are only resurfaced every 78 years on average (Asphalt Industry Alliance, 2018). Cracking and fretting (i.e. the loss of aggregate material from the road surface) are the predominant failure modes of local roads in the UK. However, automated means of detecting these two modes have had mixed success (Oliveira and Correia, 2009; Zou *et al.*, 2012; Oliveira and Correia, 2013). This is due to a number of factors including the difficulty of distinguishing cracking and fretting from the inherent road texture, the variety of road surface types within the road network and the variable weather and lighting conditions experienced in the UK (Zhang *et al.*, 2017; Brilakis and Radopoulou, 2018; Pan *et al.*, 2018). Consequently, the most common and most reliable method for the assessment of these failure modes on local roads is still by visual inspection, with its inherent subjectivity. A promising, but as yet untried, alternative is the application of geophysical methods such as ground penetrating radar (GPR), which has the potential additional benefit of being able to measure crack depth and also identify subsurface cracks. Traditional approaches only measure surface cracks. Geophysical methods have not been routinely utilised largely because the evidence base underpinning their efficacy and value for road condition assessment has to date not been sufficiently strong. GPR has been used in a wide range of other applications, for example the inspection of geological structures (Benedetto and Pajewski, 2015), surveying of critical transport infrastructure (Tosti *et al.*, 2018), and the detection and assessment of buried utilities (Cataldo *et al.*, 2014). Commercial GPR applications have also included determining the thickness of Hot Mix Asphalt (HMA) and Portland Cement Concrete (PCC) and the underlying layers (Al-Qadi and Lahouar, 2005), and therefore are recognised as having value in the road industry.

GPR is based on the classic radar principle that involves transmission of an electromagnetic wave through the material under investigation and measurement of the Time-of-Flight (ToF) of the reflected wave (Metje *et al.*, 2007). The advantages of GPR are commonly cited as the cost efficiency relative to and the possible speed of survey, and sufficient accuracy and resolution for many applications. However, there are very few studies on the feasibility of using GPR for crack detection, albeit the literature suggests that GPR with a high carrier frequency and scan resolution can fulfil the requirement for non-destructive road assessment (Birtwisle and Utsi, 2008; Utsi *et al.*, 2008; Diamanti *et al.*, 2010). This application is explored hereafter.

Some early studies showed that although GPR can prove successful for road surface crack detection, there are some challenges. For example, Ahmad *et al.* (2012) present the opportunities and limitations of using GPR as a crack detection tool. The temperature at which to utilise GPR must be above freezing to allow a sufficiently high degree of contrast in the dielectric values between the surface and cracks. This limitation was observed by Ahmad *et al.* (2012) during a field trial; however, the reason for this was not explained. This might be attributed to the crack being filled with water and hence freezing temperatures creating ice blocks with closer dielectric values to the asphalt compared with air. Also, the materials used in road construction influence the possibility for void detection within the road structure; for instance, GPR does not function well in wet clays since the GPR signals are readily absorbed by water, i.e. signal attenuation is relatively large (Rogers *et al.*, 2012). Ahmad *et al.* (2011) reported GPR measurements of asphalt specimens with uniform, i.e. saw-cut, cracks. However, these results were unsatisfactory from a commercial perspective in terms of the GPR image resolution and Signal-to-Noise Ratio (SNR). A more robust study by Diamanti *et al.* (2010) used a multiple-channel ground-coupled system for high speed road scanning. The Finite-Difference Time-Domain (FDTD) method was used to provide numerical solution for the use of the GPR in a 'forward-looking' approach. However, the approach was only tested on a single dataset and no further analysis of the FDTD data was carried out. In an alternative approach, the diffraction of the waveform has been used for road surface assessment with an oblique antenna configuration (Pennock and Jenks, 2014). This approach measured the power from each reflection angle, but it proved difficult to extract the precise location of a crack. Moreover, the crack detection work reported above did not exploit fully the potential of post-processing of the GPR image.

This paper verifies the performance of a novel automated crack detection method using a GPR system and Singular Value Decomposition (SVD) image post-processing technique to assess the detectability of pre-defined cracks in asphalt pavement slabs and assesses the effectiveness of the method in terms of the minimal detectable crack size.

Seven asphalt pavement specimens with a variety of different crack widths and shapes are screened to fully test the potential of the proposed crack detection method. The performance of the developed post-processing algorithm under different environmental and physical conditions was investigated, where the surface of the cracks was covered by 1) paper sheets 2) a thin layer of bitumen and filled with 3) fine sand and 4) water. This paper is structured as follows: Section 2 reviews the literature on the application of GPR for detecting asphalt

pavement cracks. Section 3 presents the adopted methodology, while Section 4 outlines the use of Singular Value Decomposition (SVD) for clutter reduction on GPR images and automatic data extraction. Section 5 presents the results and analysis, followed by discussions on the potential application to practice in Section 6, and conclusions are drawn in Section 7.

2   Literature Review

Automatic interpretation of GPR images has become more prevalent in recent years, but mainly aimed at detecting buried assets, especially pipes where the focus is on the identification of the hyperbola indicating the presence of a pipe. In contrast, GPR is not regularly used for crack detection in asphalt in the first place and any automatic data processing is still being developed.

2.1   GPR for Road Crack Detection

The Transport Research Laboratory (TRL) trialled GPR for crack detection (Forest and Utsi, 2004) on road pavements with a minimum of 100 mm thick asphalt surfacing. The results, verified by coring, showed that the utilised GPR system, with antennas ranging in frequency from 700 MHz to 2.5 GHz, was capable of measuring crack depths between 50 mm to 160 mm. The study also revealed that, to achieve accurate results, the survey (i.e. antenna orientation) should be conducted perpendicular to the crack, with a minimum sampling interval of 10 mm. It was concluded that variations in crack size (crack depth less than 50mm) and heterogeneity of pavement layers (e.g. a large stone in the granular layer) can lead to a false interpretation.

Birtwisle and Utsi (2008) and Utsi *et al.* (2008) reported the findings of two field trials using a multi-channel GPR for the assessment of an airport runaway, which consisted of a composite pavement (i.e. an asphalt layer overlying a concrete base). Subsurface vertical crack detection was validated by visual inspections and coring. The utilised method consisted of two crack detection heads with 1 GHz antennas, and was shown to be able to identify subsurface cracks and to measure their depth and extent. However, the majority of the identified cracks were visible surface cracks and the efficacy in identifying those that did not manifest at the surface was unknown. It should be noted also that in this study the location of the subsurface cracks was predictable prior to conducting the survey since they were found to be in close proximity to joints in the concrete slabs, crack formation in this case being a well-known phenomenon. Furthermore, the low speed of operation (1.3 km/day), due to the small sampling intervals (10 mm and 20 mm for joint and crack detection respectively) being used in an attempt to achieve higher accuracy, was a drawback of the employed method in practice.

Colagrande *et al.* (2011) investigated which GPR parameters, including power curves, absorption angle and absorption coefficients (obtained by setting the propagation velocity to 10 cm/ns), should be considered when attempting to detect the main cause(s) of deterioration of a flexible asphalt road pavement. The study collected GPR data from 40 deteriorated and newly constructed roads using 1600 MHz and 600 MHz antennas. Colagrande *et al.* (2011) concluded that similar absorption angles for damaged and undamaged roads show fatigue or thermal shrinkage as the likely cause of degradation. Dissimilarities in absorption angles, however, showed that traffic load is probably responsible for the degradation by causing uneven subgrade settlements.

Simonin *et al.* (2014), also described in Simonin *et al.* (2012), reported the findings of an experiment utilising two 3D GPR systems for detecting artificial defects in a pavement structure. Unlike traditional radar systems with one antenna, one of the 3D systems comprised eight ground-coupled antennas, each of which were operated with a frequency of approximately 1,000 MHz, while the other system consisted of 11 transmitters and 11 receivers operating at around 1,500 MHz frequency. Several different defects were simulated in a pavement structure consisting of two bituminous layers (an 80 mm thick base layer and a 60 mm thick wearing course) overlying a granular subbase. The simulated defects were placed between the bituminous layers with the following dimensions; 0.5 m × 2.0 m, 0.5 m × 0.5 m, 3.0 m × 1.0 m and 1.5 m × 2.0 m. Geotextile samples and sand (properties and thicknesses not provided) were used for simulating the defects. The results demonstrated the ability of the 3D system to capture the depth and width of defects. Tong *et al.* (2017) utilised GPR to identify concealed cracks in pavement and generated a 3D model of them using the convolutional neural network (CNN) method, with a reported zero percent identification error on 6482 tested GPR images. However, it should be noted that the size of the concealed cracks was not reported, while an average error of 5 mm was reported (showing that the crack sizes should be much larger than 5 mm). CNN is an image processing technique, which has been used for detecting pavement cracks from 2D and 3D images generated by various techniques, for example Zhang *et al.* (2016) applied it on photographic colour images and achieved around 87% accuracy, but did not apply it on real time images. Tong *et al.* (2018) used CNN to process 312 GPR images from road subgrade layers to detect defects, but the dimensions of the defects were not reported. The findings showed that it was more reliable, over 90% accuracy, than two other image processing techniques, namely Sobel edge detection and K-value clustering. However, the

comparison between the three aforementioned techniques was only conducted qualitatively using three images.

2.2   GPR application in automated road condition assessment

Recent developments in robotics and computation have enhanced automated GPR road condition assessment, in both conducting the survey and data processing. There are numerous papers on automatic detection and assessment of buried utilities using the GPR technology, for example Maas and Schmalzl (2013); Qiao *et al.* (2015); Yuan *et al.* (2018); Jazayeri *et al.* (2019); Cai *et al.* (2020); Yuan and Cai (2020), the subject of the current paper is however the application of automated GPR technology for road condition assessment. For instance, a robotic system employing image processing and GPR technologies was developed by Li *et al.* (2016) for automated pothole detection, which was able to detect over 50 different potholes with 88% accuracy.

Hugenschmidt and Fürholz (2012) described an automated acquisition system mounted on a trailer, consisting of a GPS receiver, a data acquisition system and a GPR system (the frequency used was not given). The developed system was tested solely on a bridge and no technical data, other than the physical components, was reported.

When utilising GPR for testing over an entire road network, the amount of data can cause significant operational problems, adding to the complexity of data acquisition, analysis and interpretation. Varela-González *et al.* (2014) developed a semi-automatic processing and visualisation tool to reduce the time required to analyse GPR data for road pavement thickness measurements. The processing time using three different hardware configurations for various lengths of road network, between 100 m and 20 km, was reported to be less than 30 seconds. More recently, Sukhobok *et al.* (2019) used an artificial neural network technique to automatically evaluate pavement thickness using GPR technology. The developed algorithm was trained and tested using the data gathered on a 60 km stretch of motorway. The results on detecting different layers of the pavement, but not their thicknesses, were compared with those detected manually showing no complete agreement between the two. However, the paper lacked an appropriate analysis of the results making it hard to judge the success of the developed algorithm. Pupatenko *et al.* (2019) also utilised a neural network technique to automatically identify pavement layers and boundaries using GPR images. A relatively low frequency antenna, 450 MHz, was utilised in the study. The predicted boundaries by the

developed algorithm was only compared qualitatively. Automated detection of pavement layers using GPR was also investigated by Lahouar and Al-Qadi (2008), who utilised a developed post-processing algorithm consisting of a threshold detector. The algorithm was tested using the 1 GHz air-coupled GPR antenna on a section of a road and achieved a 2.5 % average thickness error. Zhili *et al.* (2016) also utilised an automated GPR image processing technique to measure asphalt layer thickness, which was tested on ten GPR images. The results were compared with manual detection results and achieved an accuracy of up to 3.14 mm in thickness estimation, but the study failed to validate the results with any coring from the road. Some of the other studies which investigated the application of automated GPR technique for asphalt and/or pavement thickness measurements include Maser and Scullion (1992); Olhoeft and Smith (2000); Zhou *et al.* (2010); Oliveira *et al.* (2014); Liu *et al.* (2016); Wang *et al.* (2020).

A threshold approach was adopted by Uus *et al.* (2016) to process GPR data to detect significant deviations in a pavement's subsurface structure and properties. A demonstration was conducted using an 800 MHz antenna, but the results of the study were not validated as no information on the identified subsurface defects was available.

Dossi *et al.* (2015b) and Dossi *et al.* (2015a) reported on an automated GPR algorithm based on a signal phase assessment which was tested on an airport runway to detect the transition between a concrete and an asphalt layer. The study failed to demonstrate a clear application of the developed algorithm for the road condition assessment. Todkar *et al.* (2017) utilised a supervised machine learning technique named support vector machines for detecting pavement de-bonding. The result showed that the ratio between number of correctly detected de-bonding (true positive) over the total of true positive and non-detected de-bonding (false negative) was around 93% which is an interesting result. Furthermore, the authors tested the developed method during a field trial, reported in Todkar *et al.* (2018), to detect artificial defects, i.e. de-bonding modelled by inserting layers of sand, tack-free based material and geotextile into asphalt. The results of the developed support vector machines technique for de-bonding detection, reported in Todkar *et al.* (2017), were compared with three different signal processing methods, namely: Amplitude Ratio Test, Semi-Supervised Clustering Algorithm, and Random Forests technique. The study concluded that both the support vector machines and Random Forests techniques provided the best results, based on the Dice score performance index, described in Todkar *et al.* (2017).Lu *et al.* (2002) evaluated the suitability of GPR technology for automatically detecting pavement cracks and measuring their depths, through

reviewing the literature and conducting laboratory and field experiments. They concluded that the approach was not an appropriate method because of 1) the unavailability of quantitative data on measured reflected waves by commercially available GPR units, 2) the reliance on expert judgment and interpretation, and also 3) the cost. They concluded therefore that there was a need to develop a new signal processing system that would enable GPR to be used as part of an automated unit.

Previous research on post-processing for GPR images includes that from Paglieroni and Beer (2014), which contains a complicated analysis of 3D data, and Pennock and Jenks (2014), which uses the diffraction information but is insensitive to deep cracking. Various filtering methods and processes utilised in GPR processing are described by Utsi (2017), including background removal, which has been utilised in this study through SVD. SVD has been utilised widely in GPR post-processing, for example by Cagnoli and Ulrych (2001); Kim *et al.* (2007); Guo and Hesthaven (2019), however, it is not normally effective in an inhomogeneous environment such as the ground when used by its own, as stated by Smitha and Singh (2019). Narayanan *et al.* (2017) successfully utilised 2D median filtering and PSNR thresholding methods in radar holography for detecting concealed objects, with security applications. Soldovieri *et al.* (2006) reported utilisation of a horizontal filtering method combined with an inverse scattering approach for GPR images to remove background noises in an attempt to automatically locate rebar in concrete, but a fully automated process was not achieved.

This paper aims to overcome the aforementioned drawbacks of GPR in road surface crack detection, as concluded by Lu *et al.* (2002), by developing an automated GPR signal processing approach. The algorithm complexity is controlled while ensuring that the system is able to detect cracking of various depths is proposed.

3 Method

3.1 Asphalt Slabs

To examine the feasibility of GPR to detect surface cracking in pavements, seven asphalt slabs were cast. The asphalt slabs had overall dimensions of 500 mm × 500 mm × 110 mm (depth), the latter dimension being the minimum recommended thickness for the surface layer of a road pavement, e.g. Kent County Council (2000). Cracks ranging in width from 1 mm to 32 mm were created in the slabs using an actuator to apply a load of up to 70 kN (Figure 1). All cracks

penetrated the surface and the crack depth was 110 mm throughout. An example of the resulting cracked asphalt pavement is shown in Figure 2.

Figure 1: Crack simulation process using an actuator

Figure 2: One of the tested asphalt slabs

3.2   GPR Measurements

A GroundVue 3 GPR system, manufactured by Utsi Electronics (2018), with a 2 GHz antenna was deployed to collect the surface data from the asphalt slabs. A 4 GHz antenna, also

manufactured by Utsi Electronics (2018), was also tested, but the 2 GHz antenna provided a better resolution. The system consists of two parts: a Radio Frequency (RF) head that includes one transmitter and one receiver, and a controller. The RF head transmits microwave pulses through the ground and collects the reflected signals. The raw data is then passed to the controller via an external cable. The controller initialises the RF head and transfers the data to a laptop via Wi-Fi (or cable). It also contains an odometer to measure the travelling distance of the system, which is based on an encoder wheel.

All the GPR system parameters used are presented in Table 1. The sweep time defines the travel time between the transmitter-target and target-receiver and is related to the achievable resolution in the GPR image; it was set at the highest rate of 10 ns. The scan frequency determines the rate of data collection, which defines the maximum velocity. The relative permittivity (Er) is a measurement of the target's ability to hold charge and relates to the type of road material (Baker *et al.*, 2007). It should be noted that the contrast between asphalt and air is the key parameter in crack detection assuming the gaps are air-filled, while water-filled gaps generate a better defined reflection with a higher amplitude compared to air-filled cracks (Solla *et al.*, 2014). In this study, Er for the asphalt pavement was set at 6 in accordance with the findings of Paje *et al.* (2008). A GPR B-scan was produced for each test, though it was noted that it was hard to visibly identify the cracks from the B-scans and thus it was concluded that post-processing was needed to analyse the data, and this was done in each case.

Table 1: GPR system parameters

Antenna Frequency	2.2 GHz
Sweep Time	10 ns
Samples per Line[1]	256
Scan Frequency	200 Hz
Triggering	Wheel
Relative Permittivity	6

[1]Number of points per sweep

During the tests, the GPR unit was moved along the centre line of the lined slabs (the dashed line in Figure 3) at walking speed. This meant that crack detection was only attempted in the transverse direction to the travel of the GPR unit.

Figure 3: GPR unit traversing the cracked asphalt specimens

It is well known that one of the main challenges for a GPR system is the strong reflection from clutter (Temlioglu and Erer, 2016), and for surface crack detection the target signal may be completely obscured by the clutter (Van Der Merwe and Gupta, 2000; Kabourek *et al.*, 2012). Thus, clutter reduction must be applied to GPR images for any crack detection scheme. In this study, a clutter reduction method based on the popular Singular Value Decomposition (SVD) technique was used, in which the eigenvalues for background clutter were removed and then extracted to reveal the crack signal. The process was followed with a median filter to remove the random noise and further improve the Peak-Signal-to-Noise Ratio (PSNR). PSNR is the ratio of maximum possible power of a signal and the power of corrupting noise that disturbs the fidelity of its representation (Ledesma-Carrillo *et al.*, 2016).

To investigate the performance of the utilised GPR system under various conditions which simulate reality, the following different environmental and physical conditions were simulated during the trial.

- The surface of the cracks were covered by paper sheets to simulate cracks covered with leaves.

- The surface of the cracks were filled with a thin layer of bitumen, to evaluate the system's ability to detect voids or cracks which do not penetrate to the surface.

- The cracks were filled with fine sand to represent cracks filled with debris and dirt.

- Numerical modelling was utilised to model cracks filled with water as it was not possible to retain the water inside the cracks during the GPR measurements. Running water was also tried, but the data was too noisy to be utilised for post processing.

4 Road Crack Detection

One of the main challenges in GPR imaging is the strong returns from the road surface, which tend to obscure stationary targets and render crack detection and classification difficult. A GPR image (A) can be considered as a sum from three signal sources (Equation 1):

$$A = C + B + n \qquad (1)$$

where C contains the signal from the cracks, B contains the signal from the road surface (background clutter) and n is the undesired signal from other sources, such as radar error and system error. Therefore, it is vital to resolve the signal of interest (C) from the measured GPR data (A). Thus, a novel signal processing method is proposed, which has not been used before, despite its potential benefits. Figure 4 shows an overview of the processing steps adopted here.

GPR Image → Singular Value Decomposition (SVD) → 2D Median Filter → PSNR Based Crack Extraction
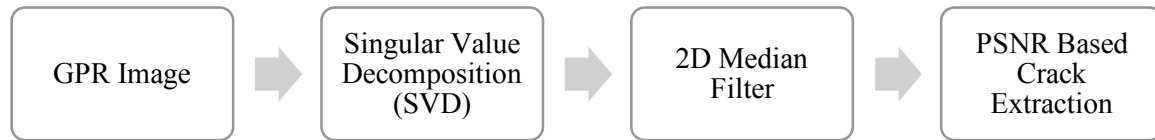
Figure 4: Proposed signal processing methodology for the automatic crack detection

4.1 Background Subtraction by SVD

SVD is a powerful tool for dealing with clutter that might otherwise obscure the crack detection signals and has been used widely for different applications (Moonen and De Moor, 1995). Its main goal is to factorise a matrix into the product of three matrices, and is used for visualising data by minimising variables, and detecting data patterns (Wall *et al.*, 2003). By evaluating the eigenvalues, SVD can separate the signal that identifies cracking from background signals. Assuming the GPR image can be represented by a rectangular matrix $\mathbf{A}_{ij}$ with dimensions of $m \times n$, where i is the travel distance index and j is the depth index and, for the GPR images obtained in this study, n is usually larger than m, the SVD of $\mathbf{A}$ can be given using Equation 2.

$$\mathbf{A} = \mathbf{US}V^* \qquad (2)$$

where $\mathbf{U}$ is an $m \times m$ unitary matrix, $\mathbf{S}$ is an $m \times n$ rectangular diagonal matrix with positive real numbers on the diagonal, and $\mathbf{V}$ is an $n \times n$ unitary matrix. Matrix $\mathbf{S} = diag(\sigma_1, \sigma_2, ... , \sigma_r)$ with $\sigma_1, \sigma_2, ... , \sigma_r \geq 0$. $\mathbf{U}$ and $\mathbf{V}$ are the left-singular and right-singular matrixes of $\mathbf{A}$, respectively. The columns of $\mathbf{U}$ and $\mathbf{V}$ are the eigenvectors of $\mathbf{AA}^*$ and $\mathbf{A}^*\mathbf{A}$, respectively, where $\mathbf{A*}$ is the conjugate transpose of matrix $\mathbf{A}$. Since $\mathbf{AA}^*$ and $\mathbf{A}^*\mathbf{A}$ are both symmetric and square, consequently

$$\mathbf{UU}^* = \mathbf{U}^*\mathbf{U} = \mathbf{I}_m \tag{3}$$

and

$$\mathbf{VV}^* = \mathbf{V}^*\mathbf{V} = \mathbf{I}_n \tag{4}$$

Where $\mathbf{I}_m$ and $\mathbf{I}_n$ are identity matrices with size m and n respectively.

Matrix $\mathbf{S}$ is an $m \times n$ matrix, and if $n \geq m$, $\mathbf{S}$ can be divided into two sub-matrices as (D, 0), where $\mathbf{D}$ is an $m \times m$ diagonal matrix and 0 is an $m \times (n - m)$ matrix of zeros. The diagonal values S_i in $\mathbf{D}$ are known as the singular values, or the square roots of the eigenvalues $\mathbf{AA}^*$ and $\mathbf{A}^*\mathbf{A}$. Then matrices $\mathbf{A}$, $\mathbf{U}$, $\mathbf{S}$ and $\mathbf{V}$ comply with Equation 5:

$$\begin{cases} \mathbf{AA}^*\boldsymbol{u}_i = \sigma_i\mathbf{u_i} \\ \mathbf{A}^*\mathbf{Av_i} = \sigma_i\mathbf{v_i} \end{cases} \quad i \leq m \tag{5}$$

where $\mathbf{u_i}$ and $\mathbf{v_i}$ are vectors of matrixes $\mathbf{U}$ and $\mathbf{V}$, respectively and σ_i is the i member of the diagonal matrix $\mathbf{S}$.

The GPR image can then be given by Equation 6.

$$\mathbf{A} = \sum_{i=1}^{m} \sigma_i\boldsymbol{u_i}\boldsymbol{v_i}^* \tag{6}$$

which is equivalent to Equation 7.

$$\mathbf{A} = \boldsymbol{a_1} + \boldsymbol{a_2} + \cdots + \boldsymbol{a_m} \tag{7}$$

where $\boldsymbol{a_i}$ are matrices with same size as $\mathbf{A}$, and are known as the modes of $\mathbf{A}$. This expansion of a matrix, as a series of sub-matrices, is one of the key features of the SVD technique (Abujarad *et al.*, 2005). In this paper, clutter reduction is achieved by identifying the key eigenvalue of SVD that relate to the background signal $\mathbf{B}$.

An example of the original GPR image and its sorted eigenvalues is presented in Figures 5 (a) and (b), which show that the first ~50 eigenvalues are dominant in terms of amplitude, whereas the remaining eigenvalues are much lower. More specifically, the first 10 eigenvalues take 91.67% of total energy, meaning that the original GPR image can be represented using only 10

eigenvalues with 8.33% loss in energy. Nevertheless, these 10 eigenvalues include the signals from the road surface, cracks and noise.
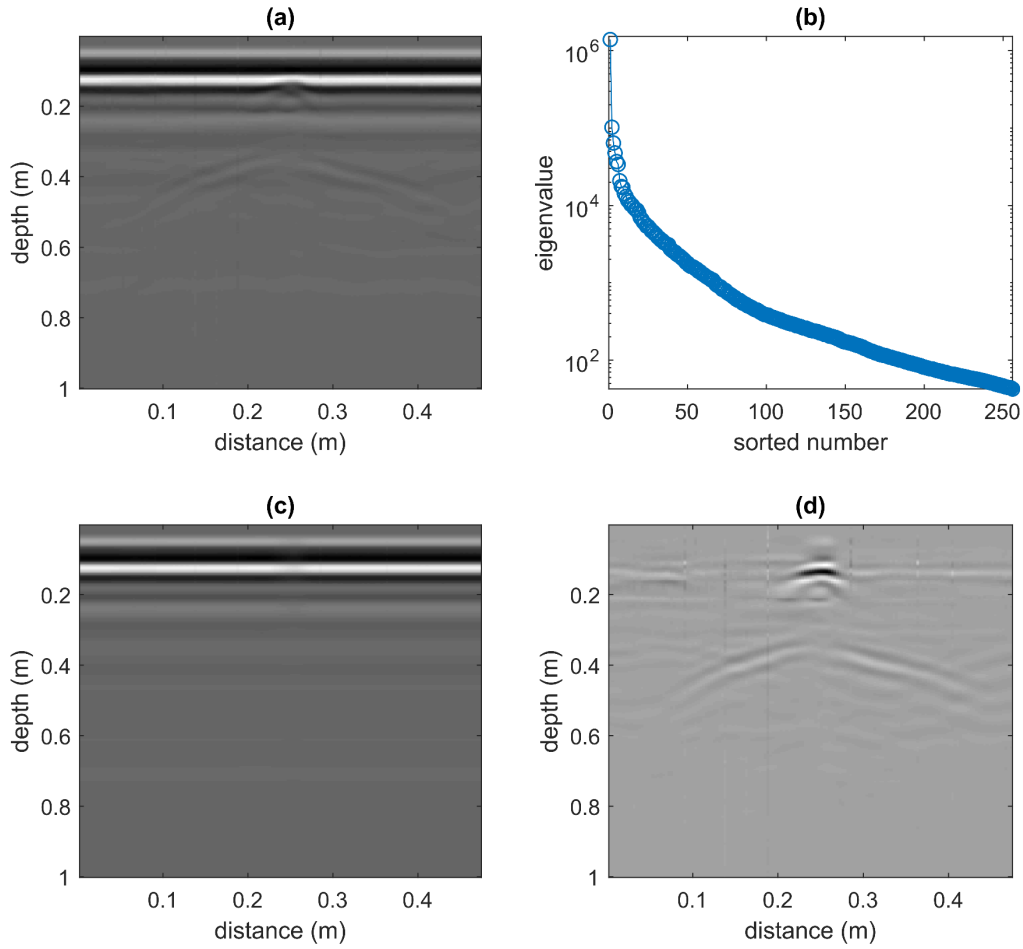
Figure 5: GPR measurement (a) original image, (b) sorted eigenvalues (c) clutter signal and (d) crack signal

The basic idea, therefore, is to split **A** into the modes according to Equation 7 so that the clutter signal is contained in the first k eigenvalues and the crack signal is in the remaining n - k eigenvalues. Thus, the next task is to find the best value of k for optimal partition in terms of PSNR, which is calculated using Equation 8, developed by Brunzell (1999):

$$\text{PSNR} = \frac{Average\ energy\ of\ crack\ signal}{Average\ energy\ of\ clutter\ signal} - 1 \qquad (8)$$

It is assumed that the clutter signal and the noise are independent and that the average energy of the clutter and noise is constant (Brunzell, 1999), whereas the energy of the target signal

includes the crack signal, clutter signal and noise. Thus, the term "-1" is used to suppress the background signal from the crack signal.

The best performance PSNR values for the entire data set were used to determine the optimised k-value, i.e. an average value of 2 was found. Examples for different k values are shown in Table 2 under PSNR(1). This shows that the highest PSNR value is at $k = 2$, reaching 417.6, and the PSNR then dramatically decays to 2.2 at $k = 4$ and remains approximately stable for the remaining k values. Therefore, it is reasonable to conclude that the first eigenvalue (also with the largest amplitude) represents the main component of the clutter signal. Thus, the cleaned GPR image $\hat{\mathbf{A}}$ can be then expressed by Equation 9.

$$\hat{\mathbf{A}} = \sum_{i=2}^{m} \sigma_i \mathbf{u_i} \mathbf{v_i}^* = \sum_{i=2}^{m} \mathbf{a}_i \tag{9}$$

The processed GPR images for $k = 2$ are shown in Figure 5 (c) for the clutter signal and in Figure 5 (d) for the crack signal. As can be seen, the clutter signal shows strong background information and constant shapes throughout its depth. In comparison, the crack signal shows a clear trajectory of the reflection whereas the strong clutter in Figure 5 (a) has been successfully removed.

Table 2: Signal-to Noise-Ratios (SNR) of Crack and Clutter signal.

SNR(1) is without filter and SNR(2) is with filter

K	1	2	3	4	5	10	25	50
PSNR(1)	11.1	417.6	31.9	2.2	3.5	0.5	2.6	3.0
PSNR(2)	11.2	440.0	25.0	1.2	2.3	0.3	0.3	0.8

4.2 Noise Reduction by 2D Median Filter

Despite the ability of the SVD process to extract the crack signal from the background clutter, it was observed that the signals still contained some random noise and spikes due to a systematic error. Thus, a further filtering process to improve the SNR was necessary. In this study, the median filter method with a size of 3 was adopted due to its simplicity of structure and powerful ability to remove the undesired noise (Yamaguchi *et al.*, 2008). It replaces the volume with the median of neighbouring pixels.

The PSNR(2) in Table 2 gives the PSNR after it was processed by a median filter, which shows that the PSNR increases to 440.0 at $k = 2$, thereby showing an improvement compared with PSNR(1). This improves the second eigenvalue of S as the dominant component for the crack signal, which, as argued above, is the value that should be applied for road crack detection. The median filter has only a slightly better PSNR performance at $k = 1$, with an improvement of 0.1. This confirms the observation that the PSNR of the crack signal in the original GPR image is not good enough for the purpose of crack detection. In addition, all PSNRs are decreased for all values of $k > 3$. This is because the dominant component of the crack signal has been filtered out, and all the other components only hold small portions of the crack signal. As a result, the median filter also enhances the noise in the GPR image, and hence the SNR values of $k > 3$ are lower than their values before applying the median filter.

Arising from the application of these two procedures, the following points need to be considered prior to utilisation of GPR images for crack detection:

- The surface of the explored area contributes most to the reflection energy recorded in a GPR image. This constitutes the first SVD eigenvalue.

- The next eigenvalue of the image represents the reflection from cracks in the road.

- All the remaining eigenvalues, in an ideal case, embody the unimportant 'noises', for example the multiple reflections from other targets and weaker reflections from smaller objects.

However, the aforementioned assumptions are primarily valid in an ideal environment, while the road surface is not truly planar in reality. In addition, it is not only the first eigenvalue that is influenced by the background clutter, but the clutter influences a finite number of eigenvalues. This also applies to the crack detection, which is characterised by several eigenvalues and not only the second.

4.3   Automatic Extraction

Another important focus of this study was the automation process for crack identification. Considering the significant difference between cracked and non-cracked areas shown in Figure 5, it is reasonable to propose that an automatic crack identification process could be achieved using this difference, and in particular, the PSNR values determined from a GPR image. From observations made over a number of GPR images, it is found that non-cracked areas have very low PSNR values, whereas cracked areas have far higher PSNR values. Based on this

assumption, a sliding window has been applied to scan the GPR image pixel by pixel in the horizontal direction. The output is a vector that contains a number of PSNR values $\mathbf{R} = [r_1, r_2, \dots r_n]$. Applying a threshold ($T$) to the PSNR values ($\mathbf{R}$), a decision vector $\mathbf{D}$ can be calculated using Equation 10.

$$\begin{cases} r_i \geq T & d_i = 1 \\ r_i < T & d_i = 0 \end{cases} \tag{10}$$

where d_i is an element of $\mathbf{D}$.

A threshold was chosen using a 'rule of thumb' observation of the obtained GPR image, which is 30 PSNR in this case. The final stage is to filter out the components in vector D that are short in duration, since some noise could also give rise to high PSNR values and filtering this out improves the overall accuracy of detection. [An example from the experimental results is shown in the next section.]

5   Experimental Results

In this section, the experimental results of crack detection using GPR measurements are presented. All seven asphalt slabs were placed in a straight line to form a total of 14 cracks/gaps (8 cracks in asphalt pavement slabs and 6 cracks represented by gaps between slabs). The relative location and width of these cracks are shown in Table 3. The GroundVue 3 GPR system was moved at walking pace across the cracks on a trolley. The GPR measurements collected during this test were simultaneously transferred to a laptop for further processing.

5.1   Effectiveness of the Post-Processing

The original GPR image is shown in Figure 6(a) with all cracks highlighted by squares and numbers. Very strong background clutter is evident in the GPR image, especially close to the surface (between 0.1 and 0.2 metres), and some random noise is displayed at various depths along the image. As discussed previously, this is because the energy of the clutter is much higher than that from the cracks and this constitutes the major element in a GPR image. As a result, most of the crack trajectories are obscured, or buried within the image, and are difficult to observe. Only cracks 8 and 13 are very clearly discernible, as both of them are wider than 30 mm (see Table 3). Although they are discernible, it is relatively hard to identify cracks 1, 4 and 5, which are between 10 mm and 20 mm wide, from the image. This degree of resolution for the crack detection is too coarse for an effective and reliable real-world application, e.g. UK Pavement Management System (UKPMS, 2009 [P 15]) requires detecting cracks larger than 2 mm.
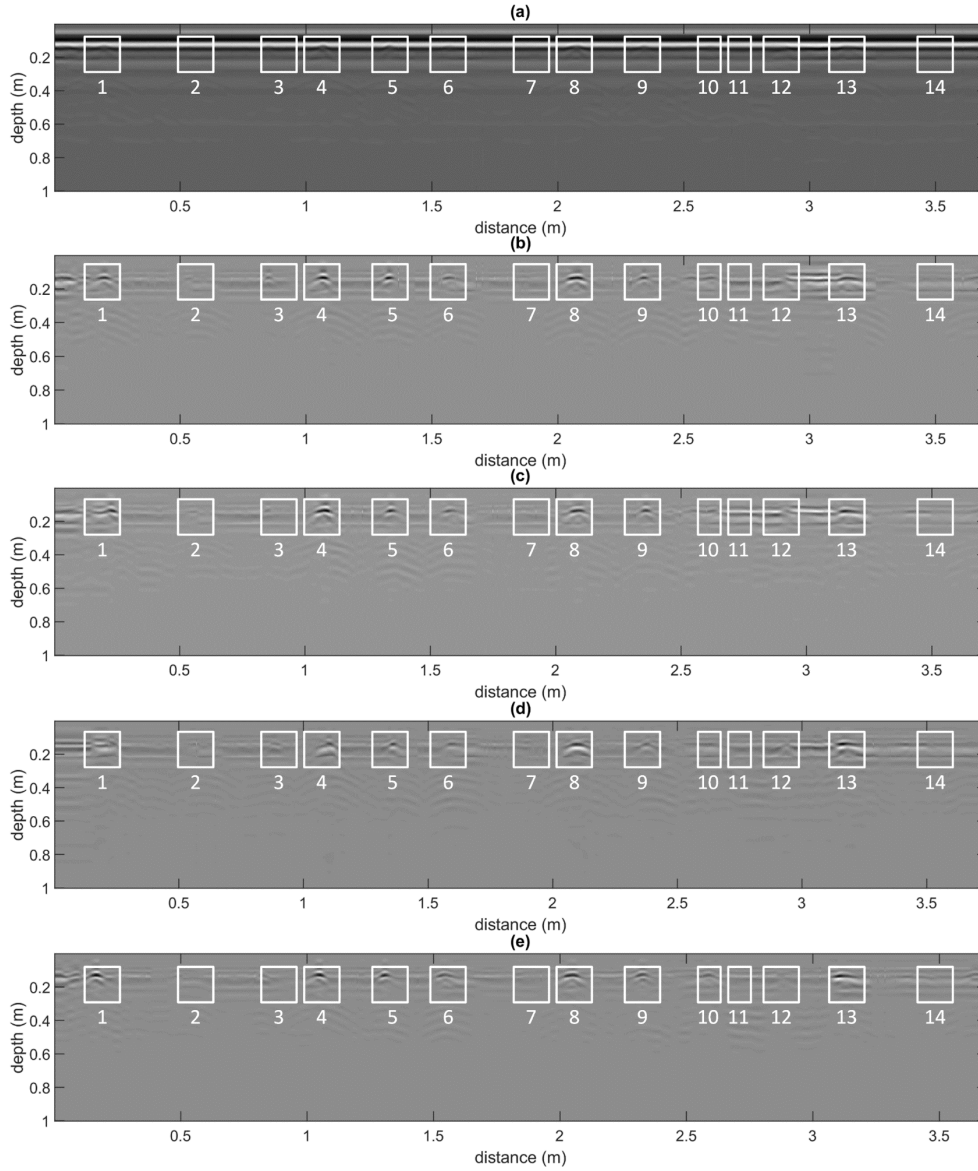
Figure 6: GPR measurement on all cracks (a) original image and processed images of cracks (b) uncovered (c) covered with paper (d) covered with thin layer of asphalt (e) filled with sand. Cracks are coded by numbers and highlighted by squares

For this reason, post-processing based on the SVD method to remove the background clutter and the application of a median filter to improve the SNR of crack signals, as described in Section 4, was carried out. The processed GPR images for various physical and environmental condition are shown in Figures 6(b-e), which show there is a significant improvement in identification of the crack trajectories when compared to Figure 6(a). More specifically, the

background clutter has now been successfully removed in Figures 6(b-e) and the large cracks (such as 1, 4, 5, 8, and 13) can be clearly distinguished from the background. The medium cracks – 6, 11 and 12, which are between 5 mm and 10 mm – can now also be observed with minimal ambiguity, and even crack 9 (a small crack that is only 3.4 mm wide) shows a discernible trajectory in the image. In contrast, it appears that the small cracks 2, 7 and 10 cannot be seen even with the proposed post-processing if one focusses on the portion of the image that appears in the red boxes. This would suggest that the limitation of detection resolution for the current system and signal processing exists at a crack width of approximately 5 mm. This leads to the detection performance of each crack by visual inspection from both the raw image and processed image recorded in Table 3, and leads to the conclusion that using a higher sweep time to enable a better resolution of the GPR image or a multiple channel GPR system to operate at different frequencies might lead to an improvement in this performance.

However, taking a broader look at the processed image in Figure 6(b) suggests that the nested hyperbolas that lie below the red boxes provide a further indication of the potential presence of cracks. Using this indicator, the cracks at points 2 and 10, when combined with the disturbance seen in the red boxes, might also suggest cracks in the asphalt. This phenomenon is also worthy of further investigation.

Table 3: Experimental results showing whether a crack is easily discernible (Good), difficult to discern (Hard) or not discernible (No)

Crack	Location (cm)	Width (mm)	Raw Image	Processed Image
1	24.0	14.4	Hard	Good
2	59.0	1.1	No	No
3	88.5	4.5	No	Hard
4	110.0	16.5	Hard	Good
5	136.5	10.1	Hard	Good
6	161.0	8.6	No	Hard
7	192.0	1.3	No	No
8	210.0	31.3	Good	Good
9	239.0	3.4	No	Good

10	258.0	4.2	No	No
11	265.0	5.7	No	Hard
12	294.0	7.0	No	Good
13	317.0	34.2	Good	Good
14	371.0	4.7	No	Hard

5.2   Automatic Detection Results

The corresponding automatic detection results, based on the data in Figure 6, are shown in Figure 7, from which it can be seen that cracks 5, 8 and 9 have relatively high PSNR peaks that can be easily identified. In contrast, cracks 2, 6, 7 and 11 have relatively low PSNR values that can hardly be detected. Furthermore, it can be observed from Figure 7 (b) that after the background reduction using the SVD technique, the PSNR value has decreased for the small cracks, possibly due to the part of the crack energy at $k = 1$ being removed by the SVD process disproportionately adversely affecting the detection of small cracks.
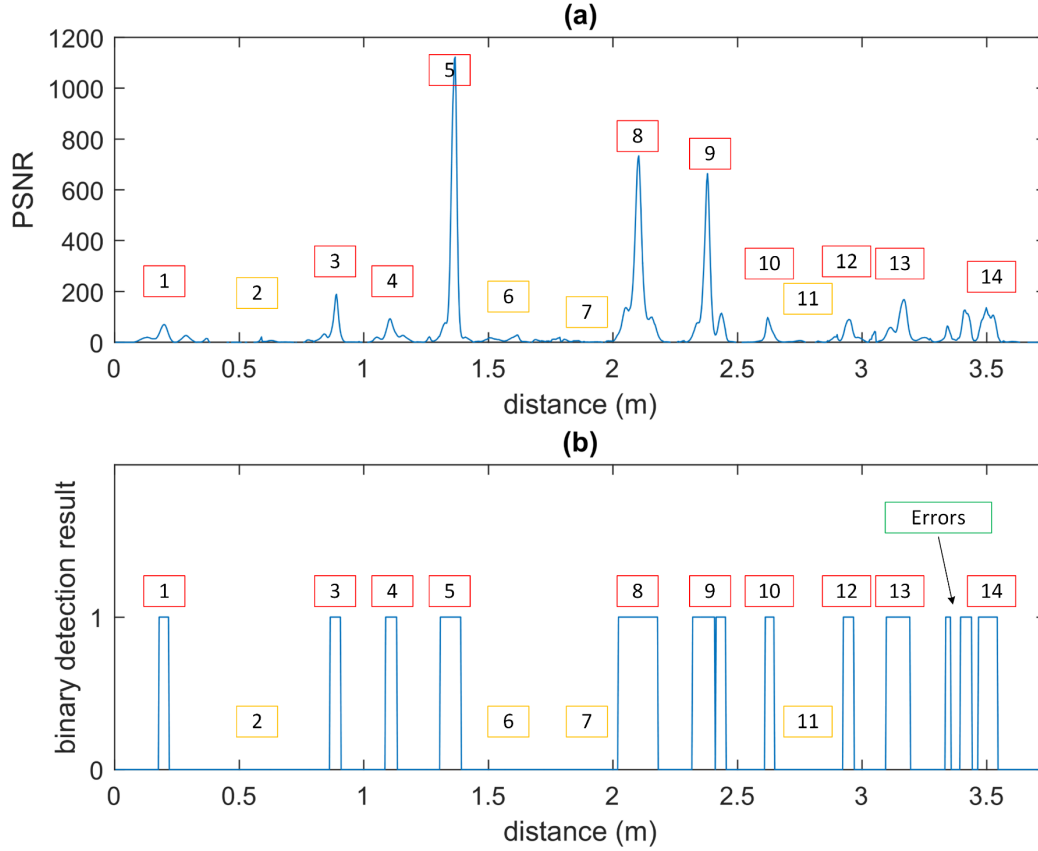
Figure 7: Automatic Crack Detection performance (a) PSNR value and (b) the binary detection results, where 1 and 0 represent positive and negative detection, respectively

There are also some detection errors near crack 14 as shown in Figure 7 (b), with two small peaks creating 'false positives'. This is because the asphalt between cracks 13 and 14 was not smooth, inducing several spikes in the PSNR value. This indicates that the roughness effects from the road surface play an important role in the GPR measurements, and discrete patches of surface roughness are themselves, of course, potential indicators of asphalt pavement degradation. Assuming that the purpose of road structure condition assessment surveys is to identify areas of potential degradation for either further detailed investigation or treatment, such an anomaly ceases to be a 'false positive' but a positive indicator of potential degradation is needed.

The developed post-processing technique was applied to the data collected under simulated environmental and physical conditions, described in Section 2.2, to assess the impact of different conditions which might occur in reality. The results are presented in Table 4.

Covering cracks with paper reduced the PSNR values (reduced energy of the crack signal) by an average of 55% for eight out of the 14 cracks, while for Crack 13 the value was nine times larger after being covered by paper. The increased value might be attributed to the variable survey conditions, including changes in vertical distance between the antenna and the crack during the survey when there is a minor change in survey route, the speed of survey and the ambient temperature affecting the speed of the electromagnetic signal and the permittivity. For the surface covered with asphalt, there was a reduction in PSNR values for 10 cracks. However, for the cracks filled with sand the data was not showing any specific trend, and it was equally divided between increased and decreased PSNR values.

The simulation of environmental and physical conditions did not show any specific trends in general and it is not possible to draw any specific conclusion. Although there were differences in PSNR as a result of the different physical conditions simulating reality, it should be noted that all PSNR values were above the threshold value and as such, those cracks which were correctly identified were identifiable independent of the environmental and physical of the cracks. This is suggesting that the developed methodology is robust and would work in practice.

Table 4: Experimental results showing PSNR values for crack detection for different environmental and physical conditions

Crack	PSNR			
	Uncovered	Covered with paper	Covered with thin layer of asphalt	Filled with sand
1	253.2	64.5	66.5	332.2
2	0.4	0.3	-0.8	10.5
3	429.7	28.5	18.7	189.1
4	364.6	231.7	12.5	49.7
5	544.9	412.5	75	1114.3
6	54.3	27.8	10.5	89.3
7	20.9	9.9	1.3	-0.3
8	194	222.4	733.7	118.3
9	388.3	397.5	664	27.8
10	45.7	51.6	16.6	60.8
11	27.3	7.8	0.08	0.7
12	10.5	88.8	22.3	112.1

|				
13	86.9	137	143.2	348.1
14	20.8	43.7	12.6	10.4

5.3   Modelling Results

ReflexW software was utilised to determine what the B-scan for a crack of different sizes, filled with air and water, would theoretically look like, using the following parameters:

- Relative permittivity – 6 for asphalt, 1 for air, 81 for water

- Frequency – 2 GHz

- Sampling – Every 2 mm

- Depth – 0.2 metres (approximately 4 ns, assuming a velocity of 0.1 m/ns)

- Noise – Exponential fluctuations with average inhomogeneities of 0.01 metres in both X and Z directions, and a variance of +/- relative permittivity of 2

All the cracks involved in the laboratory tests, listed in Table 3, were simulated. The results of this modelling are presented in Figure 8, which confirms the experimental findings that only cracks larger than 5 mm are detectable with confidence using the utilised GPR system. Furthermore, the modelling shows that the water-filled cracks are more accentuated than the air-filled cracks, as expected considering the huge contrast in relative permittivity, i.e. 81 for water compared to 1 for air. However, there is a relatively small change in responses from any cracks less than 4 mm in width. It seems that the utilised 2 GHz antenna can identify cracks larger than 4 mm in width with the presence of water; however, cracks larger than 5 mm in width are identifiable for both air and water.
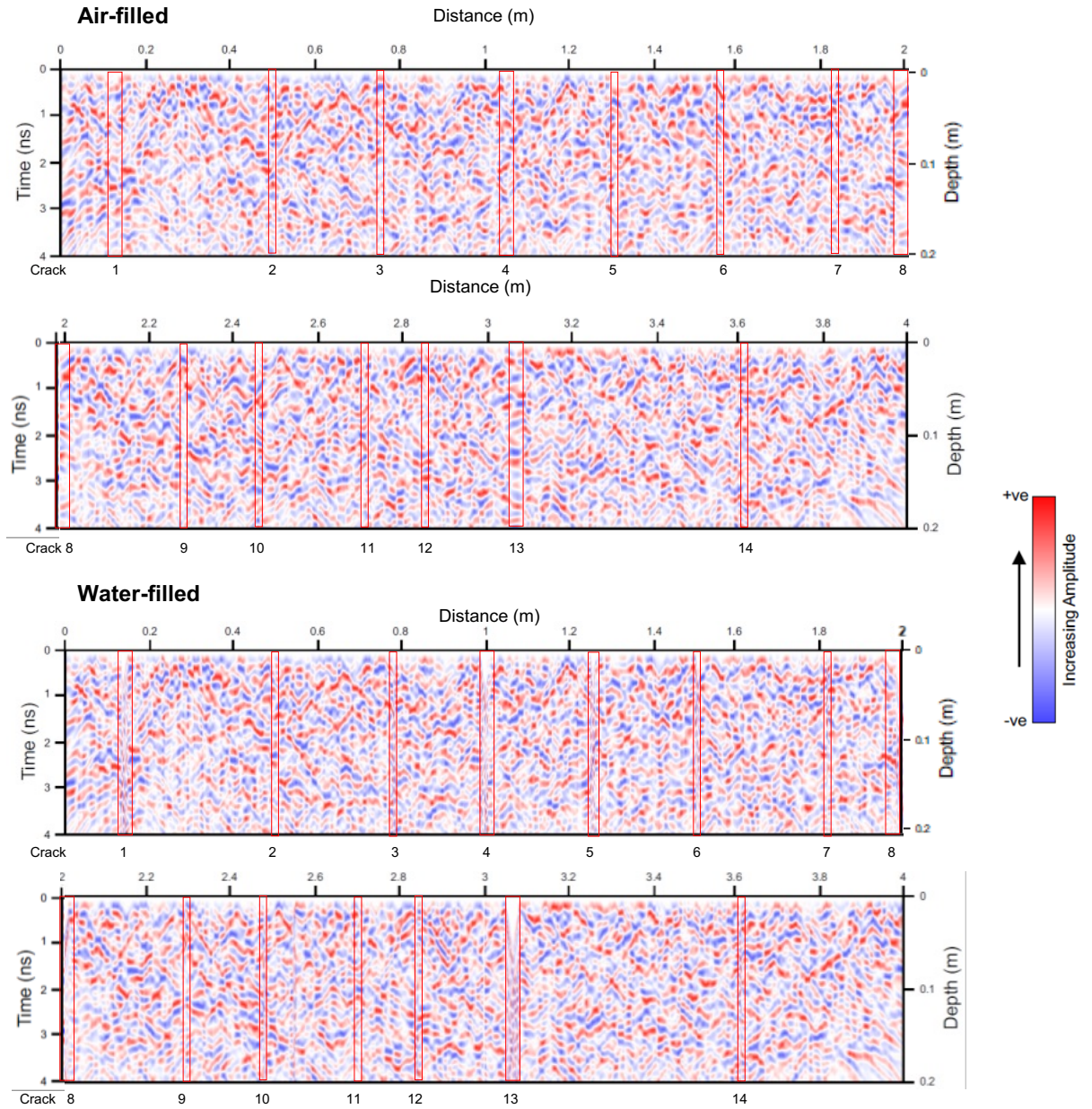
Figure 8: ReflexW software modelling results along the profile for cracks filled with air and water, identifiable cracks are highlighted

6 Potential Application to Practice

It is evident that, combining visual scrutiny of the processed GPR image and the automatic crack detection plots, only two cracks remained undetectable (these being cracks of 1.3 mm and 1.1 mm width), and one of these was shown to exhibit nested hyperbolas towards the base of the processed GPR image which might provide a weak indicator of cracking and worthy of

marking as a 'watch' if no immediate detailed surveying is planned, or a point for further detailed investigation if it is. Despite improving most 'crack signals' using the adopted post-processing methods, it was also observed that the energy of signals related to small cracks appeared to be reduced after this process. Future work should therefore include further investigation of the background reduction technique such that it enhances (relative to other contributions to the GPR signal) rather than diminishes the energy of small cracks. For instance, a more robust approach can be achieved by considering the PSNR data as a time series, which can be processed with algorithms such as the peak detection or change point detection techniques (Aminikhanghahi *et al.*, 2018). The study reported in here focussed on small scale samples, with a high degree of control on the size of the cracks and also the repeatability. Future work should expand the demonstration of the system to different types of cracks and to test the developed algorithm on a larger data set and in collaboration with practitioners to evaluate the influence of the survey methodology which is currently used in practice.

Nevertheless, the findings provide encouragement for the application of GPR, alongside other survey techniques, e.g. laser scanning, infrared thermography (Plati *et al.*, 2014; Li *et al.*, 2018; Li *et al.*, 2019), on a robotic cart that could be deployed overnight on cordoned of lengths of road as part of a minimally-disruptive programme of routine surveying. The results, when post-processed and examined by the surveyor, and combined with local knowledge (those responsible for road maintenance often have an understanding of where potential problems might occur, perhaps backed up by reports from the public), would therefore be of value in informing subsequent maintenance decisions: no further action before the next routine survey, further detailed surveying or planned maintenance activity to repair the surface. Taking this argument further, the further detailed surveying and/or maintenance activity could itself be conducted using drones or surface mounted robots at times when disruption to traffic is minimal (e.g. overnight) (Richardson *et al.*, 2017; Self-Repairing Cities, 2019).

7   Conclusions

This paper presents an experimental study of the use of a GPR system for road crack detection. In contrast to previous studies (Ahmad *et al.*, 2011; Ahmad *et al.*, 2012; Pennock and Jenks, 2014), the results have shown that using a commercial GPR system combined with novel processing techniques, cracks in asphalt pavements can be detected with confidence, and considerably better resolution in terms of the crack width. Experiments were carried out using

a GroundVue 3 GPR system with a 2 GHz antenna on seven asphalt slabs containing 14 cracks and simulated cracks, giving a total length of around 3.5 m. A Singular Value Decomposition method was applied to the resulting data to remove the strong background clutter in the GPR image, followed by a median filter to remove the random noise. The experimental results indicate that the first eigenvalue of a GPR image relates to the background clutter, while the second eigenvalue can be used as the 'crack signal', i.e. can be used to identify vertical cracking in the asphalt pavement.

The paper demonstrates that the processed GPR image enables far better visual crack detection irrespective of the simulated conditions (cracks filled with sand to simulate debris and dust, cracks covered with paper to simulate leaves on the road and cracks covered with a layer of asphalt to simulate those cracks which have not penetrated to the surface) than is possible from using the raw GPR image. It also demonstrates that the automatic detection method provides significant additional clarity. Together they therefore have shown a considerable enhancement in the confidence in the use of GPR for this application, contrary to previous experience. In the 3.5 m long experimental section, only one 'false positive' reading, attributed to the effect of surface roughness, was obtained and this in itself points to road surface degradation worthy of future investigation. Combining visual scrutiny of the processed GPR image and the automatic crack detection plots, only two narrow cracks (of 1.1-1.3 mm in width) remained completely undetectable, and one of these exhibited nested hyperbolas on the processed GPR image providing a weak indicator of cracking. The detected cracks were shown to be detectable irrespective of the physical conditions simulated, suggesting that the developed methodology is robust for use in practice. The findings provide encouragement to those seeking to apply GPR, alongside other survey techniques, for example those being researched for use on a robotic cart that could be deployed for minimally-disruptive overnight surveying. Combining the results with local knowledge would help to inform subsequent maintenance decisions and maintenance operations, which might themselves be effected using robotic means.

It was noted that although the post-processing methods improved most 'crack signals', the energy of signals related to small cracks appeared to be reduced. Further work to mitigate or reverse this effect is therefore warranted.

8   Data Availability

Some or all data, models, or code that support the findings of this study are available from the corresponding author upon reasonable request.

9   Acknowledgements

10   References

Abujarad, F., G. Nadim and A. Omar (2005). Clutter reduction and detection of landmine objects in ground penetrating radar data using singular value decomposition (SVD). Proceedings of the 3rd International Workshop on Advanced Ground Penetrating Radar, 2005. IWAGPR 2005., Delft, The Netherlands, IEEE.

Ahmad, N., H. Lorenzl and M. Wistuba (2011). Crack detection in asphalt pavements-how useful is the GPR? 6th International Workshop on Advanced Ground Penetrating Radar (IWAGPR), 2011, Aachen, Germany, IEEE.

Ahmad, N., M. Wistuba and H. Lorenzl (2012). GPR as a crack detection tool for asphalt pavements: possibilities and limitations. 14th International Conference on Ground Penetrating Radar (GPR), 2012 Shanghai, China, IEEE.

Al-Qadi, I. and S. Lahouar (2005). "Measuring layer thicknesses with GPR–Theory to practice." Construction and building materials **19**(10): 763-772.

Aminikhanghahi, S., T. Wang and D.J. Cook (2018). "Real-time change point detection with application to smart home time series data." IEEE Transactions on Knowledge and Data Engineering **31**(5): 1010-1023.

Asphalt Industry Alliance (2018). Annual Local Authority Road Maintenance (ALARM). Bristol, UK, Asphalt Industry Alliance (AIA)**:** 20.

Baker, G.S., T.E. Jordan and J. Pardy (2007). "An introduction to ground penetrating radar (GPR)." Special Papers-Geological Society of America **432**: 1.

Benedetto, A. and L. Pajewski (2015). Civil engineering applications of ground penetrating radar, Springer.

Birtwisle, A. and E. Utsi (2008). The use of ground penetrating radar to detect vertical subsurface cracking in airport runways. Proceedings of the 12th International Conference on Ground Penetrating Radar (GPR2008), Birmingham, UK.

Brilakis, I. and S. Radopoulou (2018). Improving Road Asset Condition Monitoring. 2016 Transportation Research Arena, Warsaw, Poland.

Brunzell, H. (1999). "Detection of shallowly buried objects using impulse radar." IEEE Transactions on Geoscience and Remote sensing **37**(2): 875-886.

Cagnoli, B. and T.J. Ulrych (2001). "Singular value decomposition and wavy reflections in ground-penetrating radar images of base surge deposits." Journal of Applied Geophysics **48**(3): 175-182.

Cai, J., J. Jeon, H. Cai and S. Li (2020). "Fusing Heterogeneous Information for Underground Utility Map Generation Based on Dempster-Shafer Theory." Journal of Computing in Civil Engineering **34**(3): 04020013.

Cataldo, A., R. Persico, G. Leucci, E. De Benedetto, G. Cannazza, L. Matera and L. De Giorgi (2014). "Time domain reflectometry, ground penetrating radar and electrical resistivity tomography: A comparative analysis of alternative approaches for leak detection in underground pipes." NDT & E International **62**(Supplement C): 14-28.

Colagrande, S., D. Ranalli and M. Tallini (2011). "Ground penetrating radar assessment of flexible road pavement degradation." International Journal of Geophysics **2011**: 1-11.

Diamanti, N., D. Redman and A. Giannopoulos (2010). A study of GPR vertical crack responses in pavement using field data and numerical modelling. 13th International Conference on Ground Penetrating Radar (GPR), 2010, Lecce, Italy, IEEE.

Dossi, M., E. Forte and M. Pipan (2015a). "Application of attribute-based automated picking to GPR and seismic surveys." Proceedings of the 2015 GNGTS, Trieste: 17-19.

Dossi, M., E. Forte and M. Pipan (2015b). Auto-picking and phase assessment by means of attribute analysis applied to GPR pavement inspection. 2015 8th International Workshop on Advanced Ground Penetrating Radar (IWAGPR).

Forest, R. and V. Utsi (2004). Non destructive crack depth measurements with ground penetrating radar. Proceedings of the Tenth International Conference on Grounds Penetrating Radar, GPR 2004., Delft, The Netherlands, IEEE.

Guo, M. and J.S. Hesthaven (2019). "Data-driven reduced order modeling for time-dependent problems." Computer Methods in Applied Mechanics and Engineering **345**: 75-99.

Hugenschmidt, J. and P. Fürholz (2012). ATRAS-An automated GPR system for data acquisition and storage for roads and bridges. 14th International Conference on Ground Penetrating Radar (GPR), 2012 Shanghai, China, IEEE.

Jazayeri, S., A. Saghafi, S. Esmaeili and C.P. Tsokos (2019). "Automatic object detection using dynamic time warping on ground penetrating radar signals." Expert Systems with Applications **122**: 102-107.

Kabourek, V., P. Černý and M. Mazánek (2012). "Clutter Reduction Based on Principal Component Analysis Technique for Hidden Objects Detection." Radioengineering **21**(1).

Kent County Council (2000). "Road Pavement Design Guide." from https://www.kent.gov.uk/__data/assets/pdf_file/0012/13035/Making-it-Happen-Road-pavement-design-guide-July-2000.pdf.

Kim, J.-H., S.-J. Cho and M.-J. Yi (2007). "Removal of ringing noise in GPR data by signal processing." Geosciences Journal **11**(1): 75-81.

Lahouar, S. and I.L. Al-Qadi (2008). "Automatic detection of multiple pavement layers from GPR data." NDT & E International **41**(2): 69-81.

Ledesma-Carrillo, L.M., M. Lopez-Ramirez, E. Cabal-Yepez, J. Ojeda-Castaneda, C. Rodriguez-Donate and R.A. Lizarraga-Morales (2016). FPGA-based reconfigurable unit for image encryption using orthogonal functions. International Conference on Electronics, Communications and Computers (CONIELECOMP), 2016, Cholula, Mexico, IEEE.

Li, H., C. Chou, L. Fan, B. Li, D. Wang and D. Song (2018). Robotic Subsurface Pipeline Mapping with a Ground-penetrating Radar and a Camera. 2018 IEEE/RSJ International Conference on Intelligent Robots and Systems (IROS), Madrid, Spain, IEEE.

Li, S., C. Yuan, D. Liu and H. Cai (2016). "Integrated Processing of Image and GPR Data for Automated Pothole Detection." Journal of Computing in Civil Engineering **30**(6): 04016015.

Li, W., M. Burrow, N. Metje, Y. Tao and G. Ghataora (2019). "A Novel Processing Methodology for Traffic-Speed Road Surveys Using Point Lasers." IEEE Transactions on Intelligent Transportation Systems: 1-12.

Liu, H., R. Birken and M. Wang (2016). "Automatic pavement layer identification with multichannel ground penetrating radar at traffic speed." Journal of Applied Remote Sensing **10**(4): 046023.

Lu, J.J., X. Mei and M. Gunaratne. (2002). "Development of an automatic detection system for measuring pavement crack depth on Florida roadways." from http://www.fdot.gov/research/completed_proj/summary_rd/fdot_bb884_rpt.pdf.

Maas, C. and J. Schmalzl (2013). "Using pattern recognition to automatically localize reflection hyperbolas in data from ground penetrating radar." Computers & Geosciences **58**: 116-125.

Maser, K.R. and T. Scullion (1992). "Automated pavement subsurface profiling using radar: case studies of four experimental field sites." Transportation Research Record **1344**(1992): 148-154.

Metje, N., P.R. Atkins, M.J. Brennan, D.N. Chapman, H.M. Lim, J. Machell, J.M. Muggleton, S. Pennock, J. Ratcliffe, M. Redfern, C.D.F. Rogers, A.J. Saul, Q. Shan, S. Swingler and A.M. Thomas (2007). "Mapping the Underworld – State-of-the-art review." Tunnelling and Underground Space Technology **22**(5–6): 568-586.

Moonen, M. and B. De Moor (1995). SVD and Signal Processing, III: Algorithms, Architectures and Applications, Elsevier.

Narayanan, R.M., S.A. Wilson and M. Rangaswamy (2017). "Sparsely Sampled Wideband Radar Holographic Imaging for Detection of Concealed Objects." Progress in Electromagnetics Research B **72**(1): 67–93.

Olhoeft, G. and S. Smith (2000). Automatic processing and modeling of GPR data for pavement thickness and properties, SPIE.

Oliveira, D.B., D.A.G. Vieira, A.C. Lisboa and F. Goulart (2014). "A well posed inverse problem for automatic pavement parameter estimation based on GPR data." NDT & E International **65**: 22-27.

Oliveira, H. and P.L. Correia (2009). Automatic road crack segmentation using entropy and image dynamic thresholding. 2009 17th European Signal Processing Conference, Glasgow, UK, IEEE.

Oliveira, H. and P.L. Correia (2013). "Automatic road crack detection and characterization." IEEE Transactions on Intelligent Transportation Systems **14**(1): 155-168.

Paglieroni, D.W. and N.R. Beer (2014). Spatially Assisted Down-Track Median Filter for GPR Image Post-Processing. U.S. Patent. USA, Lawrence Livermore National Security LLC **US8854249B2**.

Paje, S., M. Bueno, F. Terán, U. Viñuela and J. Luong (2008). "Assessment of asphalt concrete acoustic performance in urban streets." The Journal of the Acoustical Society of America **123**(3): 1439-1445.

Pan, Y., X. Zhang, G. Cervone and L. Yang (2018). "Detection of Asphalt Pavement Potholes and Cracks Based on the Unmanned Aerial Vehicle Multispectral Imagery." IEEE Journal of Selected Topics in Applied Earth Observations and Remote Sensing **11**(10): 3701 - 3712.

Pennock, S.R. and C.H.J. Jenks (2014). Road surface and pavement condition assessment by high frequency GPR diffraction. International Conference on Ground Penetrating Radar (GPR), 2014 15th, Brussels, Belgium, IEEE.

Plati, C., P. Georgiou and A. Loizos (2014). "Use of infrared thermography for assessing HMA paving and compaction." Transportation Research Part C: Emerging Technologies **46**: 192-208.

Pupatenko, V., Y. Sukhobok, L. Verkhovtsev and G. Stoyanovich (2019). "Automation of contrast media boundary detection when processing GPR data." IOP Conference Series: Earth and Environmental Science **403**: 012205.

Qiao, L., Y. Qin, X. Ren and Q. Wang (2015). "Identification of buried objects in GPR using amplitude modulated signals extracted from multiresolution monogenic signal analysis." Sensors **15**(12): 30340-30350.

Richardson, R., R. Fuentes, T. Chapman, M. Cook, J. Scanlan and L. Zhibin (2017). Robotic and Autonomous Systems for Resilient Infrastructure. UK-RAS White Papers© UK-RAS.

Rogers, C.D.F., T. Hao, S.B. Costello, M.P.N. Burrow, N. Metje, D.N. Chapman, J. Parker, R.J. Armitage, J.H. Anspach and J.M. Muggleton (2012). "Condition assessment of the surface and buried infrastructure–A proposal for integration." Tunnelling and Underground Space Technology **28**: 202-211.

Self-Repairing Cities. (2019). "Zero Streetworks in cities by 2050." Retrieved 25/01/2019, from http://selfrepairingcities.com/.

Simonin, J., V. Baltazart, P. Hornych, X. Dérobert, E. Thibaut, J. Sala and V. Utsi (2014). Case study of detection of artificial defects in an experimental pavement structure using 3D GPR systems. 15th International Conference on Ground Penetrating Radar (GPR), 2014, Brussels, Belgium, IEEE.

Simonin, J., V. Baltazart, P. Hornych, J. Kerzrého, X. Dérobert, S. Trichet, O. Durnd, J. Alexandre and A. Joubert (2012). "Detection of debonding and vertical cracks with non destructive techniques during accelerated pavement testing." Advances in pavement design through full-scale accelerated pavement testing. Taylor & Francis Group, London: 121-133.

Smitha, N. and V. Singh (2019). "Decluttering Using Wavelet Based Higher Order Statistics and Target Detection of GPR Images." Sensing and Imaging **20**(1): 2.

Soldovieri, F., R. Persico, E. Utsi and V. Utsi (2006). "The application of inverse scattering techniques with ground penetrating radar to the problem of rebar location in concrete." NDT & E International **39**(7): 602-607.

Solla, M., S. Lagüela, H. González-Jorge and P. Arias (2014). "Approach to identify cracking in asphalt pavement using GPR and infrared thermographic methods: Preliminary findings." NDT & E International **62**: 55-65.

Sukhobok, Y., L. Verkhovtsev and Y. Ponomarchuk (2019). Automatic Evaluation of Pavement Thickness in GPR Data with Artificial Neural Networks. IOP Conference Series: Earth and Environmental Science, IOP Publishing.

Temlioglu, E. and I. Erer (2016). "Clutter removal in ground-penetrating radar images using morphological component analysis." IEEE Geoscience and Remote Sensing Letters **13**(12): 1802-1806.

Todkar, S.S., C.L. Bastard, V. Baltazart, A. Ihamouten and X. Dérobort (2018). Comparative Study of Classification Algorithms to Detect Interlayer Debondings within Pavement Structures from Step-Frequency Radar Data. IGARSS 2018 - 2018 IEEE International Geoscience and Remote Sensing Symposium.

Todkar, S.S., C.L. Bastard, A. Ihamouten, V. Baltazart, X. Dérobert, C. Fauchard, D. Guilbert and F. Bosc (2017). Detection of debondings with Ground Penetrating Radar using a machine learning method. 2017 9th International Workshop on Advanced Ground Penetrating Radar (IWAGPR).

Tong, Z., J. Gao and H. Zhang (2017). "Recognition, location, measurement, and 3D reconstruction of concealed cracks using convolutional neural networks." Construction and Building Materials **146**: 775-787.

Tong, Z., J. Gao and H. Zhang (2018). "Innovative method for recognizing subgrade defects based on a convolutional neural network." Construction and Building Materials **169**: 69-82.

Tosti, F., L.B. Ciampoli, F. D'Amico, A.M. Alani and A. Benedetto (2018). "An experimental-based model for the assessment of the mechanical properties of road pavements using ground-penetrating radar." Construction and Building Materials **165**: 966-974.

UKPMS (2009). The UKPMS User Manual 2009, Volume 2: Visual Data Collection for UKPMS, Chapter 7: Coarse Visual Inspection (CVI) J. Wallis. Wokingham, UK, UK Pavement Management System (UKPMS)**:** 71.

Utsi, E., A. Birtwisle and J. Cook (2008). Detection of subsurface reflective cracking using GPR. 12th International Conference and Exhibition of Structural Faults & Repair, Edingburgh, Engineering Technics Press.

Utsi, E.C. (2017). Ground penetrating radar: theory and practice. Oxford, United Kingdom, Butterworth-Heinemann.

Utsi Electronics. (2018). "Groundvue 3 - Multi Channel." Retrieved 5/12/18, from http://www.utsielectronics.co.uk/groundvue-3-multi-channel.

Uus, A., P. Liatsis, G. Slabaugh, A. Anagnostis, S. Roberts and S. Twist (2016). Trend deviation analysis for automated detection of defects in GPR data for road condition surveys. 2016 International Conference on Systems, Signals and Image Processing (IWSSIP).

Van Der Merwe, A. and I.J. Gupta (2000). "A novel signal processing technique for clutter reduction in GPR measurements of small, shallow land mines." IEEE transactions on Geoscience and Remote Sensing **38**(6): 2627-2637.

Varela-González, M., M. Solla, J. Martínez-Sánchez and P. Arias (2014). "A semi-automatic processing and visualisation tool for ground-penetrating radar pavement thickness data." Automation in Construction **45**: 42-49.

Wall, M.E., A. Rechtsteiner and L.M. Rocha (2003). Singular value decomposition and principal component analysis. A practical approach to microarray data analysis, Springer**:** 91-109.

Wang, S., S. Zhao and I.L. Al-Qadi (2020). "Real-Time Density and Thickness Estimation of Thin Asphalt Pavement Overlay During Compaction Using Ground Penetrating Radar Data." Surveys in Geophysics **41**(3): 431-445.

Yamaguchi, T., S. Nakamura, R. Saegusa and S. Hashimoto (2008). "Image- based crack detection for real concrete surfaces." IEEJ Transactions on Electrical and Electronic Engineering **3**(1): 128-135.

Yuan, C. and H. Cai (2020). "Spatial reasoning mechanism to enable automated adaptive trajectory planning in ground penetrating radar survey." Automation in Construction **114**: 103157.

Yuan, C., S. Li, H. Cai and V.R. Kamat (2018). "GPR Signature Detection and Decomposition for Mapping Buried Utilities with Complex Spatial Configuration." Journal of Computing in Civil Engineering **32**(4): 04018026.

Zhang, A., K.C.P. Wang, B. Li, E. Yang, X. Dai, Y. Peng, Y. Fei, Y. Liu, J.Q. Li and C. Chen (2017). "Automated Pixel-Level Pavement Crack Detection on 3D Asphalt Surfaces Using a Deep-Learning Network." Computer-Aided Civil and Infrastructure Engineering **32**(10): 805-819.

Zhang, L., F. Yang, Y.D. Zhang and Y.J. Zhu (2016). Road crack detection using deep convolutional neural network. IEEE International Conference on Image Processing (ICIP), 2016, Phoenix, AZ, USA, IEEE.

Zhili, C., O.O. Olatubosun, Z. Hui and S. Renjie (2016). Automatic detection of asphalt layer thickness based on Ground Penetrating Radar. 2016 2nd IEEE International Conference on Computer and Communications (ICCC).

Zhou, H., S. Li and J. Zhu (2010). Automatic layer-interface detection of pavement based on Matched Filter. 2010 6th International Conference on Wireless Communications, Networking and Mobile Computing, WiCOM 2010.

Zou, Q., Y. Cao, Q. Li, Q. Mao and S. Wang (2012). "CrackTree: Automatic crack detection from pavement images." Pattern Recognition Letters **33**(3): 227-238.